ARTICLES

Excited-State Distortion of Rhenium(III) Sulfide and Selenide Clusters

Thomas G. Gray, Christina M. Rudzinski, Emily E. Meyer, and Daniel G. Nocera*

Department of Chemistry, Massachusetts Institute of Technology, 6-335, Cambridge, Massachusetts 02139-4307

Received: July 1, 2003; In Final Form: November 15, 2003

The deactivation process for the excited-state decay of hexanuclear rhenium(III) sulfide and selenide clusters, $[Re_6S_8]^{2+}$ and $[Re_6Se_8]^{2+}$, has been identified from temperature-dependent photophysical measurements and electronic structure calculations. Plots of ln k_{nr} vs T^{-1}, where k_{nr} is the nonradiative decay rate constant, yield activation energies for nonradiative energy dissipation ranging from 1221 to 1933 cm^{-1}, after allowing for low-temperature tunneling. Nonlocal density-functional calculations, with varying proportions of Hartree−Fock exchange, well approximate the experimental 9 K emission maximum of the representative compound $(Bu_4N)_4[Re_6S_8Cl_6]$. The adiabatic potential energy surface of the luminescent, lowest energy triplet excited state is substantially fixed by symmetry, and the calculations provide quantitative characterization of its features. Notably, the experimental activation energies for a $D_{4h}(^3B_{1g}) \rightarrow O_h(^1A_{1g})$ excited-state decay process have the same magnitude as zero-point corrected energies of well-defined PES local maxima. The results herein further contribute to rhenium chalcogenide clusters' stature as the most thoroughly characterized luminescent metal−metal bonded clusters known.

Introduction

The hexanuclear rhenium(III) chalcogenide clusters $[Re_6Q_8]^{2+}$ (Q = S, Se, Te) have elicited considerable recent attention,[1−3] not least for their luminescence.[4−11] Excitation with ultraviolet or blue light generates bright red emission. Luminescence lifetimes last for microseconds, and emission quantum yields range from 1 to 23% in fluid solution.[4] Their luminescence is quenched by atmospheric oxygen, suggesting applications to singlet-O_2 generation[12] and optical sensor technology.[13,14]

We have recently completed a broad-based temperature-dependence study of $[Re_6S_8]^{2+}$ and $[Re_6Se_8]^{2+}$ luminescence.[15] The results of this examination indicate a triplet excited state largely confined to the six rhenium(III) ions common to all such clusters. Excited-state properties are unaffected by the core chalcogenides, whether sulfur or selenium, and are only moderately sensitive to exocluster ligands. Measurements on 24 clusters show that the approximate energy gap law is observed in fluid solution at room temperature, and in the solid phase at 298 and 77 K. Emission bandwidth analysis and quantum-chemical calculations implicate nine distinct vibrational modes in the nonradiative decay of the halide clusters $[Re_6S_8X_6]^{4-}$ (X = Cl, Br, I). Interestingly, a like conclusion holds for $[Re_6Q_8(CN)_6]^{4-}$ (Q = S, Se) species; the higher-energy oscillators associated with cyanide are largely uninvolved in nonradiative relaxation.

Herein, we characterize the physical transformation leading to vibrational deactivation. A temperature-dependence study of $[Re_6Q_8]^{2+}$ emission lifetimes yields an activation barrier for nonradiative decay. An Arrhenius-type behavior is found, if proper account is taken of low-temperature tunneling. We have investigated the lowest triplet-state adiabatic potential energy surface along which this transformation occurs, with approximate density-functional theory.[16,17] Calculations employing generalized-gradient approximations (GGA) and hybrid functionals were scrutinized. Time-dependent computations[18,19] were undertaken to estimate luminescence energies. We propose a new hybrid functional, incorporating a 24.3% admixture of Hartree−Fock exchange, fitted to recover the low-temperature emission maximum of $(Bu_4N)_4[Re_6S_8Cl_6]$. The results so obtained reveal that the activated process for triplet-to-singlet decay is a $D_{4h}(^3B_{1g}) \rightarrow O_h(^1A_{1g})$ distortion. The transformation is consistent with nonradiative decay measurements herein, and with previous work.[4,15] Excited-state decay is interpreted with a model where normal modes largely centered on the hexanuclear rhenium core induce nonradiative relaxation.

Experimental and Computational Details

Hexanuclear rhenium(III) chalcogenide clusters were prepared according to published procedures and gave satisfactory ^1H NMR and ^{31}P NMR (where applicable) spectra and mass spectral analyses.[2,20] Spectroscopic-grade solvents (Burdick and Jackson) were used for electronic absorption and emission and photophysical measurements. Solvents were used as received, though care was taken to minimize exposure to moisture.

Temperature-dependent emission spectra and excited-state lifetimes were collected on solid samples under vacuum using a front-face solid sample holder aligned at 45° to the incident beam. Samples were thermally regulated from 9 to 345 K using an Air Products (Allentown, PA) CSA-202E cryogenic refrig-

* Corresponding author. E-mail: nocera@mit.edu.

10.1021/jp0358937 CCC: $27.50
Published on Web 03/23/2004

eration system equipped with a DMX-1 vacuum shroud interface, a DE−202 expander module, and an Air Products 1R02A air-cooled compressor. Powdered solid samples are compressed into a 5 mm × 5 mm × 2 mm well in a machined copper block mounted to the sample head of the DE−202. Indium foil was used between the block and the expander to ensure good thermal conductivity. Samples were kept for at least 10 min prior to data acquisition to allow thermal equilibration. The temperature was varied using a Scientific Instruments 9600-5 temperature controller with a resistive heating element, and was monitored with a gold-calomel thermocouple remounted at the end of an expander module by Advanced Research Systems (St. Charles, IL). The DMX-1 vacuum shroud interface had two Suprasil windows on adjacent sides, allowing excitation light to strike the sample and emitted light to be collected at a 90° to the incident beam. Temperature-dependent data were collected in both directions (high to low, and low to high) to ensure reproducibility.

Time-resolved luminescence data were measured using a Coherent Infinity XPO tunable laser that has previously been described.[15] The resultant third harmonic 355 nm radiation was passed thorough Type I tunable XPO, in this case to produce the excitation wavelength of 460 nm (SHG was not required). Solution and solid sample emission was collected at a 90° angle to the incident excitation beam through a SPEX Triax 320 monochromator. Solid samples were positioned at 45° to the incident beam. Signal was detected between 720 and 750 nm, depending on the emission maximum of the sample, by a Hamamatsu R928 PMT and signal averaged for approximately 1000 scans with a LeCroy 9384CM 1 GHz Digital Oscilloscope. Detection instrumentation was controlled using National Instruments v4.0 software and data were fit using Origin 6.0.

Spin-unrestricted density-functional theory computations were performed within the Gaussian98 program suite.[21] DFT calculations employed the Becke nonlocal exchange functional,[22] with the correlation functional of Perdew.[23,24] Direct methods were used for self-consistent field convergence. Because of the size of the clusters, relativistic effective core potentials and the standard double-ζ 5s, 5p, 5d, and 6s contracted orbitals of Hay and Wadt,[25] augmented by the diffuse p-functions of Couty and Hall,[26] were used for rhenium. These potentials incorporate heavy-metal relativistic effects. The 6-31G+(d) basis of Pople and co-workers was applied to all other atoms.[27,28] The default "extrafine" grid was used in all DFT computations. Harmonic vibrational frequencies were calculated analytically.

Results and Discussion

Photophysical Measurements. Figure 1a demonstrates variations in temperature-dependence of k_{obs} upon axial ligand substitution for the halide clusters **1**−**3**. Figures 1b and 1c compare the effects of symmetry on k_{obs} resulting from face-bridging and axial ligand substitution. Attempts to fit the data assuming only classical behavior with an Arrhenius fit, failed,[29] and it was impossible to determine the appropriate temperature regime to analyze. This circumstance indicates a finite tunneling contribution at very low temperatures.

Equations developed by Englman[30] relating changes in k_{obs} to temperature, enable calculating both the barrier crossing activation energy, and ν, the preexponential factor that quantifies the "frequency of incidence over the barrier." This general method encompasses both quantum mechanical and classical behavior, unlike the more common Arrhenius method, which neglects the tunneling contribution. In this generalized case, the transmission probability, $W(T)$ contains two terms. The first

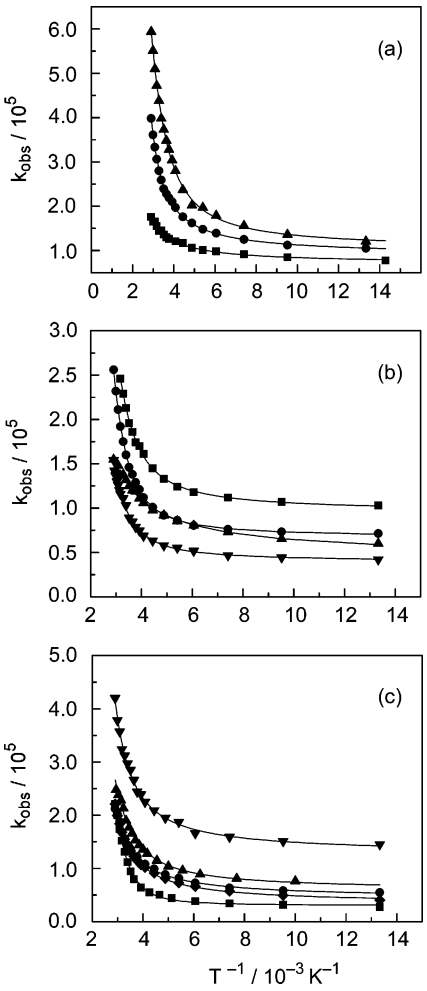

Figure 1. Temperature dependence of k_{obs} for the solid state: (a) $[Re_6S_8X_6]^{2-}$ (X = halide) clusters **1** (■, $(Bu_4N)_4[Re_6S_8Cl_6]$), **2** (●, $(Bu_4N)_4[Re_6S_8Br_6]$), and **3** (▲, $(Bu_4N)_4[Re_6S_8I_6]$); (b) $[Re_6Se_8]^{2+}$ exo-phosphine clusters **5** (▲, $[Re_6Se_8(PEt_3)_6]I_2$), **11** (●, *trans*-$[Re_6Se_8(PEt_3)_4I_2]$), **12** (■, *cis*-$[Re_6Se_8(PEt_3)_4I_2]$), and (▼, (Bu_4N)[*mer*-$Re_6Se_8(PEt_3)_3Br_3$]); and (c) $[Re_6S_8]^{2+}$ exo-phosphine clusters **4** (■, $[Re_6S_8(PEt_3)_6]Br_2$), **6** (●, $[Re_6S_8(PEt_3)_5Br]Br$), **7** (◆, *trans*-$[Re_6S_8(PEt_3)_4Br_2]$), **8** (▲, *cis*-$[Re_6S_8(PEt_3)_4Br_2]$), and **9** (▼, (Bu_4N)[*mer*-$Re_6S_8(PEt_3)_3Br_3$]). The solid curves correspond to fits using eq 3.

term, resulting from the integration of $W(T)$ using a harmonic approximation, is given by the following expression:

$$\frac{W(T)}{\nu} = \left(\frac{2\pi k_B T}{\hbar\omega} - 1\right)^{-1} (e^{-E_a/k_B T} - e^{-2\pi E_a/\hbar\omega}) \qquad (1)$$

which represents the contribution of tunneling effects. The second term denotes the contribution of the classical probability for overcoming a barrier of height E_a:

$$\frac{W(T)}{\nu} = e^{-E_a/k_B T} \qquad (2)$$

Equation 2 describes nonradiative decay exhibiting pure Arrhenius behavior. Combining eqs 1 and 2 and simplifying yields an expression for the overall temperature-dependence of the observed rate constant

$$k_{obs}(T) = k_o + \nu\left(\frac{2\pi k_B T}{\hbar\omega} - 1\right)^{-1}\left(\frac{2\pi k_B T}{\hbar\omega} e^{-E_a/k_B T} - e^{-2\pi E_a/\hbar\omega}\right) \qquad (3)$$

where k_B is the Boltzmann constant, and the constant k_o

TABLE 1: Variable-Temperature Lifetime Data for the Hexanuclear Rhenium(III) Chalcogenide Clusters[a]

no.	compound	E_a [b] (cm^{-1})	ν[b] (10^7 s^{-1})
1	$(Bu_4N)_4[Re_6S_8Cl_6]$	1509	1.16
2	$(Bu_4N)_4[Re_6S_8Br_6]$	1819	4.98
3	$(Bu_4N)_4[Re_6S_8I_6]$	1665	5.96
4	$[Re_6S_8(PEt_3)_6]Br_2$	1933	15.65
5	$[Re_6Se_8(PEt_3)_6]I_2$	1899	4.20
6	$[Re_6S_8(PEt_3)_5Br]Br$	1786	1.94
7	*trans*-$[Re_6S_8(PEt_3)_4Br_2]$	1757	2.64
8	*cis*-$[Re_6S_8(PEt_3)_4Br_2]$	1620	2.90
9	(Bu_4N)[*mer*-$Re_6S_8(PEt_3)_3Br_3$]	1619	3.11
10	$[Re_6Se_8(PEt_3)_5I]I$	1676	6.08
11	*trans*-$[Re_6Se_8(PEt_3)_4I_2]$	1890	8.25
12	*cis*-$[Re_6Se_8(PEt_3)_4I_2]$	1828	6.04
13	$(Bu_4N)_4[Re_6S_8(CN)_6]$	1221	0.53
14	$(Bu_4N)_4[Re_6Se_8(CN)_6]$	1415	0.19

[a] E_a is the activation energy and ν is the preexponential frequency factor; parameters were measured in solid state. [b] Error in E_a is ±20%; error in ν is ±25%.

subsumes temperature-independent contributions to the observed rate. Since $k_r \ll k_{nr}$ [15] and remains constant with temperature, the temperature dependence of k_{obs} directly reflects the activated temperature dependence associated with nonradiative decay. In the high-temperature limit ($k_BT \gg \hbar\omega$), the classical contribution controls the transition rate, while quantum tunneling dominates in the low-temperature limit ($T \rightarrow 0$). If the effects of tunneling are negligible at an accessible temperature, eq 2 can be used to determine E_a by a linear fit of ln k_{obs} against T^{-1} in this classical region. In this study, however, the temperature range falls almost entirely within a regime where quantum tunneling makes a significant contribution to the excited-state decay, necessitating the use of eq 3.

Table 1 lists activation energies and frequency factors determined by fitting the data with eq 3 (shown by solid lines in Figures 1). Experimentally determined E_a values for all Re_6 clusters range from 1500 to 1900 cm^{-1}, except for the $[Re_6Q_8(CN)_6]^{4+}$ (Q = S, Se) clusters (**13** and **14**), which show lower activation energies of 1221 and 1415 cm^{-1}, respectively. The activation energy is largely independent of changes in symmetry and ligands (both axial and face-bridging); no trends are observed among the data. The preexponential factor dominates the observed changes in k_{obs}. The frequency factors are on the order of 10^7 s^{-1} for each cluster, and they increase monotonically along the series Cl < Br < I (for clusters **1**−**3**). Similarly, it appears that the face-bridging ligand is also correlated to ν as is seen in the data for clusters **4**−**5** and **13**−**14**, given in Table 1. Here the values of ν for the sulfur-containing clusters are consistently higher by approximately a factor of 4. Changes in symmetry have a lesser influence on ν.

Computations. The structures of the ground- and lowest-energy emitting states of $[Re_6S_8Cl_6]^{4-}$ and its triplet-state adiabatic potential energy surface were explored using the exchange functional of Becke[22] with the correlation functional of Perdew,[23,24] (BP86), and a variant, incorporating partial Hartree−Fock exchange. Such hybrid functionals are believed to mitigate the self-interaction error associated with approximate exchange-correlation functionals.[31] Hybrid exchange-correlation functionals have better reproduced forward and reverse activation barriers,[32] experimental ground-state spin densities,[33,34] NMR chemical shifts,[35] and other experimental observables.[36,37] We have calibrated a new hybrid functional by fitting the fraction of HF exchange that recovers the 9 K emission maximum. A 50% inclusion of Hartree−Fock exchange yielded a negative triplet-to-singlet transition energy, indicating a triplet ground state, despite all experimental evidence.[1−8,15] For this reason, calculations using greater proportions of HF exchange were not pursued.

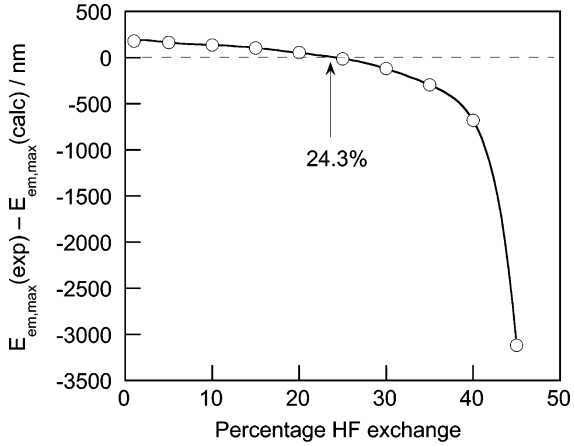

Figure 2. Polynomial fit of the difference between calculated and observed $^3B_{1g} \rightarrow {}^1A_{1g}$ energy gap for $[Re_6S_8Cl_6]^{4-}$ in the D_{4h}-symmetric geometry of the triplet state, optimized without HF exchange. The minimum error between experimental and calculated emission energies is shown by the arrow (percentage HF exchange = 24.3%).

The energy and composition of the LUMO → HOMO transition of $(Bu_4N)_4[Re_6S_8Cl_6]$, were determined for 1−45% HF exchange admixtures (Table 1, Supporting Information). Hartree−Fock exchange was introduced on a percentage basis, so that the proportions of nonlocal and HF exchange added to unity; hybridization of the correlation functional was not attempted. In all cases, the $^3B_{1g}$ state is the lowest-energy triplet. All time-dependent calculations employ the D_{4h}-symmetric geometry of the $^3B_{1g}$ state optimized from spin-unrestricted BP86 calculations. Time-dependent calculations without exact exchange encountered severe convergence difficulties, but addition of 1% HF exchange gave rapid convergence. Calculations with 1% HF exchange indicate an exclusively LUMO → HOMO emissive transition, but increasing the fraction of HF exchange admits contributions from transitions between nonfrontier orbitals. These added contributions reflect the influence of higher-energy determinants in the converged Kohn−Sham wave function. They may partially compensate for counterion effects, which are otherwise neglected.

Figure 2 plots the difference between calculated $^3B_{1g} \rightarrow {}^1A_{1g}$ transition energies for varying HF exchange admixtures within a time-dependent density-functional formalism[38] and the experimental 9 K luminescence maximum for $(Bu_4N)_4[Re_6S_8Cl_6]$. This low-temperature emission maximum was chosen to minimize contributions from vibrationally excited states. Superimposed is a best-fit eighth-order polynomial, itself insignificant except for the real root at ∼24.3% HF exchange. This is the fraction of exact exchange that best recaptures the low-temperature emission energy. We adopt the acronym B(24.3HF)P86 to denote Becke's exchange functional, modified to include 24.3% HF exchange and 75.7% nonlocal exchange, with Perdew's 1986 correlation functional.

Figure 3 presents the spin-unrestricted, optimized structure of the singlet ground state of $[Re_6S_8Cl_6]^{4-}$ obtained from the B(24.3HF)P86 and BP86 (reference) calculations; Table 2 summarizes calculated metrics. Full O_h symmetry was imposed on the geometry optimization of singlet $[Re_6S_8Cl_6]^{4-}$, a prototype of the series of clusters. Calculations using the hybrid B(24.3HF)P86 and nonhybrid BP86 functionals reproduce crystallographic Re−Re bond lengths[2] to within 0.062 Å; Re−S distances are within 0.050 Å of experiment. Metal−chloride bond lengths differ by as much as 0.070 Å from the experimental

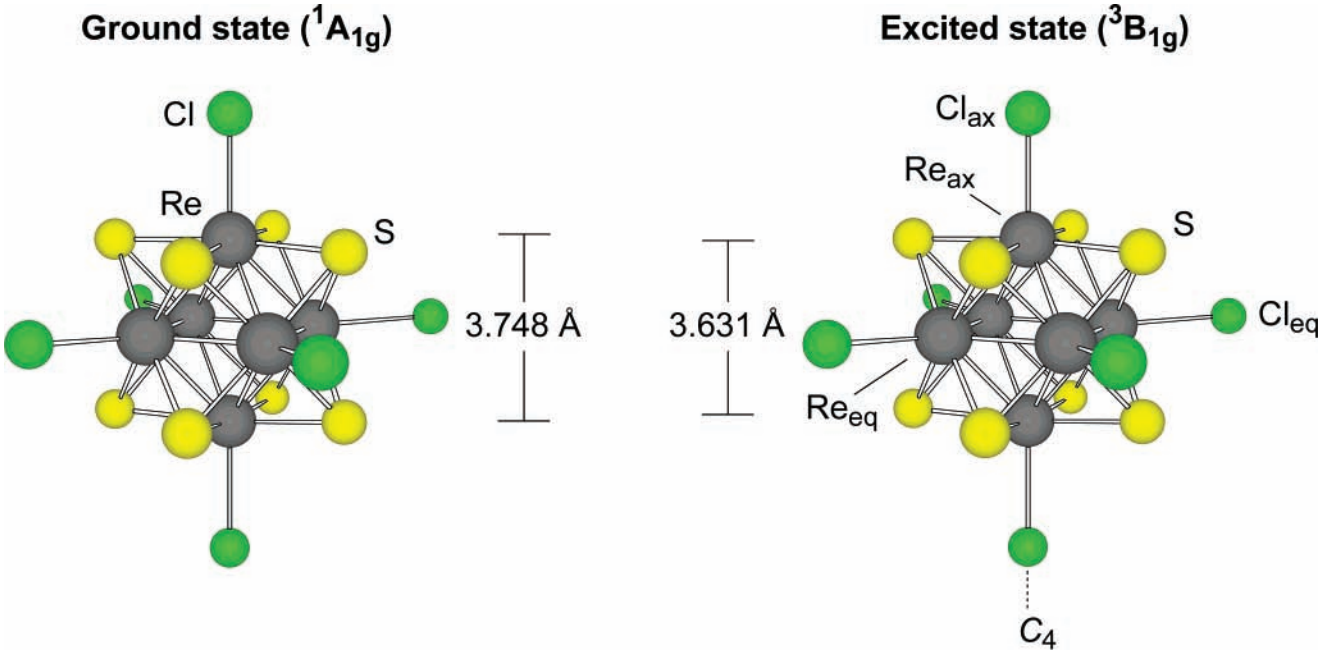

Figure 3. Calculated geometries of (a) singlet and (b) triplet $[Re_6S_8Cl_6]^{4-}$ with the correlation functional of Becke and the exchange functional of Perdew, and with the same functional hybridized with a 24.3% admixture of HF exchange with 75.7% nonlocal exchange.

TABLE 2: Calculated and Experimental Interatomic Distances in $[Re_6S_8Cl_6]^{4-}$ in Its Lowest-Energy Excited State and Ground State

$^1B_{1g}$ (O_h) Ground State			
interatom	BP86	B(24.3HF)P86	Experimental
Re−Re	2.650 Å	2.619 Å	2.601(4) Å
Re−S	2.449 Å	2.428 Å	2.403(9) Å
Re−Cl	2.521 Å	2.496 Å	2.451(1) Å
Cl-trans-Cl	8.782 Å	8.696 Å	8.58(1) Å

$^3B_{1g}$ (D_{4h}) Excited State		
interatom	BP86	B(24.3HF)P86
$Re_{ax}-Re_{eq}$	2.615 Å	2.637 Å
$Re_{eq}-Re_{eq}$	2.661 Å	2.678 Å
$Re_{ax}-Cl_{ax}$	2.449 Å	2.495 Å
$Re_{eq}-Cl_{eq}$	2.519 Å	2.495 Å
$Re_{ax}-S$	2.404 Å	2.451 Å
$Re_{eq}-S$	2.403 Å	2.420 Å
Cl_{eq}−trans-Cl_{eq}	8.872 Å	8.778 Å
$Cl_{ax}-Cl_{ax}$	8.754 Å	8.660 Å

value. The hybrid B(24.3HF)P86 functional better reproduces crystallographic bond lengths by 0.013 Å, on a mean absolute deviation basis, than does nonhybrid BP86. The fidelity of the calculated geometries compares favorably with available optimizations of rhenium compounds using effective core potentials[39−41] and all-electron basis sets.[42,43]

Triplet-state geometry optimizations afforded the D_{4h}-symmetric structure shown in Figure 3; harmonic frequency calculations confirmed these to be energy minima. The lower symmetry of the triplet cluster is in agreement with standard Jahn−Teller theory.[44,45] Figure 3 shows the calculated triplet to be tetragonally compressed along the C_4 axis. Re−Cl bonds along the C_4 contract by not more than 2.86% of their calculated singlet-state values. Axial Re−centroid lengths shrink by 0.021Å (1.2%); equatorial Re−Re bonds shrink by 0.022 Å (1.1%), both relative to calculated singlet-state values. The volume of the rigorous S_8 cube in singlet clusters is nearly unchanged on distorting to the triplet state.

Figure 4 depicts a thermodynamic cycle that affords another estimate of the phosphorescence energy of triplet species at 0

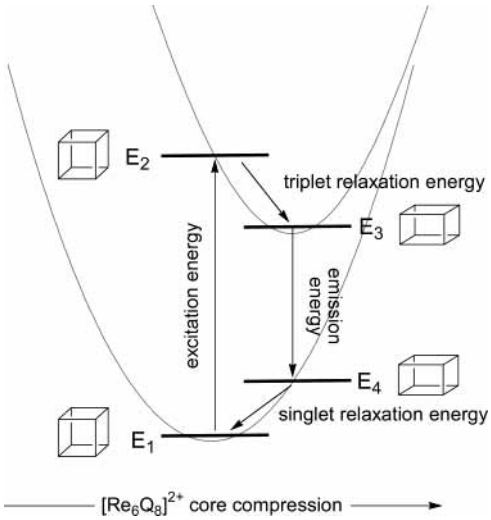

Figure 4. A thermodynamic cycle for calculation of energy changes accompanying $[Re_6S_8Cl_6]^{4-}$ distortion into various geometries of ground and lowest-energy excited states.

K. Four relevant energy levels are defined by the geometry-optimized equilibrium structures of singlet (ground state) and triplet (excited) $[Re_6S_8Cl_6]^{4-}$. At room- and lower temperatures, the singlet cluster accesses the triplet geometry continuously, and the triplet cluster likewise samples the singlet structure. The term "Franck−Condon triplet" connotes the spin-triplet cluster in the O_h geometry of the singlet; the "Franck−Condon singlet" is the ground-state cluster in the D_{4h}-triplet geometry. Table 3 collects BP86-calculated sums of electronic and thermal free energies; all are corrected for zero-point energy. It is significant that the relaxation energy separating the excited-state equilibrium structure from the Franck−Condon geometry (at constant spin multiplicity) is ∼1300 cm^{-1} range, which is similar to the ∼1500−2000 cm^{-1} activation barrier measured from temperature-dependent lifetimes. This result leads us to conclude that excited → ground-state interconversion in this cluster series is determined by the tetragonal → octahedral excited-state distortion.

TABLE 3: $[Re_6S_8Cl_6]^{4-}$ Energies Calculated within the Thermodynamic Scheme of Figure 4[a]

energy levels	E (hartrees)	ΔE (hartrees)	ΔE (kJ/mol)	ΔE (cm^{-1})	$E_{em,max}$ 9 K (cm^{-1})
E_1	−6423.31263223	0.00000000	0.0000	0	
E_2	−6423.23057223	0.08206000	215.6	18021	
E_3	−6423.23658197	0.07605026	199.8	16701	
E_4	−6423.30700990	0.00562233	14.77	1235.0	
$E_{em,max}$(calcd)	0.07042793	0.07042793	185.0	15467	11500

[a] All are calculated with the nonlocal exchange functional of Becke and the correlation functional of Perdew, and are corrected for zero-point energy.

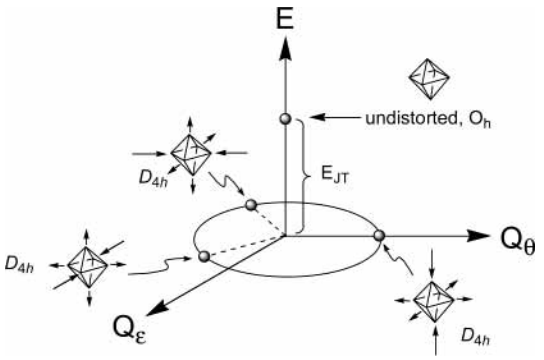

Figure 5. Diagram of the salient landmarks on the adiabatic potential energy surface of the lowest energy, $^3[Re_6S_8Cl_6]^{4-}$ ($^3B_{1g}$), excited state.

Triplet $[Re_6S_8Cl_6]^{4-}$, having a singly occupied e_g HOMO − 1, experiences an E⊗e Jahn−Teller distortion.[46] The adiabatic potential energy surface is 3-fold-symmetric (Figure 5) with equivalent minima equally displaced from a common center, along a normal coordinate accounting for compression of the octahedral core. The local minima correspond to tetragonal clusters, distorted along each of three mutually perpendicular axes, all with D_{4h} symmetry. Their stabilization energy relative to the Franck−Condon triplet is E_{JT}. Table 3 indicates this stabilization energy to be 15.8 kJ mol^{-1}. Transitions states, also D_{4h}-symmetric, connect the three minima; their geometries are averages of the neighboring minimum-energy structures. The remaining points on the least-motion pathway connecting all minima have D_{2h} symmetry.

Single-point energy calculations of the excited-state local minima indicate an activation free energy of 3.65 kJ mol^{-1} for interconversion among degenerate triplet geometries (not corrected for zero-point energies). This value is not far different from the energy of the Franck−Condon triplet, and both have the same magnitude as the activation energy found from temperature-dependent emission lifetime measurements. These calculations indicate excited-state potential energy surface landmarks with energies the same magnitude as the experimental activation barriers for nonradiative decay. They further indicate that energetic barriers to distortion, including the O_h structure of the ground-state cluster, are moderate, a finding consistent with the small nonradiative decay activation barriers encountered experimentally.

In summary, the structural transformation accompanying excited-state decay of $[Re_6Q_8]^{2+}$ clusters has been identified. Nonlocal and hybrid density-functional calculations on a representative cluster, $[Re_6S_8Cl_6]^{4-}$, indicate a low-lying, D_{4h}-symmetric triplet state. The triplet structure is tetragonally flattened compared to that of the singlet ground state. The activation energy for excited → ground state interconversion is determined experimentally to be ∼1500−2000 cm^{-1} for all members of the cluster series; this result is consistent with the energy calculated for a tetragonal → octahedral distortion of the electronically excited cluster species. The activation energy is independent of the clusters' local symmetry, and is insensitive both to exocluster ligands and face-capping chalcogenides. These findings agree with photophysical measurements that show that the nonradiative decay of $[Re_6S_8X_6]^{4-}$ (X = Cl, Br, I) clusters is governed by low-energy vibrations (<500 cm^{-1}) localized within the Re_6 metal core. From the results presented here, it is logical that these core localized vibrations will be excited as the $[Re_6Q_8]^{2+}$ clusters relax from the long-lived excited state to the ground state. The distortion governing the six metals of the $[Re_6Q_8]^{2+}$ clusters is akin to that observed for the six ligands of octahedral mononuclear complexes subject to Jahn−Teller instabilities, especially those involving copper.[45,47,48]

The foregoing results extend the emerging database surrounding metallocluster photoprocesses. A profusion of $[Re_6Q_8]^{2+}$ clusters is available,[20,49−55] with changeable apical ligand spheres and the choice of in-core sulfide or selenide. The predictable emission properties[4,15] of these many clusters suggest the findings herein to be general, and hence applicable to the controlled design of these emitting clusters for a variety of light-emitting applications.

Acknowledgment. We thank R. H. Holm (Harvard University) and R. K. Szilagyi (Stanford University) for useful discussions. T.G.G. acknowledges a postdoctoral fellowship (2002−2004) from the National Institutes of Health. C.M.R. was a Corning Fellow. Research at MIT was supported by a grant from the AFOSR (F49620-98-1-0203) and a Collaborative Research in Chemistry grant from the National Science Foundation (CHE 02-09898).

Supporting Information Available: Calculated $^3B_{1g} \rightarrow 1A_{1g}$ transition data for $[Re_6S_8Cl_6]^{4-}$ as a function of HF exchange inclusion (Table S1). This information is available free of charge via the Internet at http://pubs.acs.org.

References and Notes

(1) Long, J. R.; Williamson, A. S.; Holm, R. H. *Angew. Chem., Int. Ed. Engl.* **1995**, *34*, 226.
(2) Long, J. R.; McCarty, L. S.; Holm, R. H. *J. Am. Chem. Soc.* **1996**, *118*, 4603.
(3) Saito, T. *J. Chem. Soc., Dalton Trans.* **1999**, *97*, 1999.
(4) Gray, T. G.; Rudzinski, C. M.; Nocera, D. G.; Holm, R. H. *Inorg. Chem.* **1999**, *38*, 5932.
(5) Yoshimura, T.; Umakoshi, K.; Sasaki, Y.; Ishizaka, S.; Kim, H.-B.; Kitamura, N. *Inorg. Chem.* **2000**, *39*, 1765.
(6) Yoshimura, T.; Ishizaka, S.; Sasaki, Y.; Kim, H.-B.; Kitamura, N.; Naumov, N. G.; Sokolov, M. N.; Fedorov, V. E. *Chem. Lett.* **1999**, 1121.
(7) Yoshimura, T.; Ishizaka, S.; Umakoshi, K.; Sasaki, Y.; Kim, H.-B.; Kitamura, N. *Chem. Lett.* **1999**, 697.
(8) Guilbaud, C.; Deluzet, A.; Domercq, B.; Moliné, P.; Coulon, C.; Boubekeur, K.; Batail, P. *Chem. Commun.* **1999**, 1867.
(9) Arratia-Pérez, R.; Hernández-Acevedo, L. *J. Chem. Phys.* **1999**, *110*, 2529.
(10) Arratia-Pérez, R.; Hernández-Acevedo, L. *J. Chem. Phys.* **1999**, *111*, 168.
(11) Arratia-Pérez, R.; Hernández-Acevedo, L. *J. Chem. Phys.* **2003**, *118*, 7425.

(12) Jackson, J. A.; Newsham, M. D.; Worsham, C.; Nocera, D. G. *Chem. Mater.* **1996**, *8*, 558.
(13) Ghosh, R. N.; Baker, G. L.; Ruud, C.; Nocera, D. G. *Appl. Phys. Lett.* **1999**, *75*, 2885.
(14) Demas, J. N.; DeGraff, B. A.; Coleman, P. B. *Anal. Chem.* **1999**, *71*, 793A.
(15) Gray, T. G.; Rudzinski, C. M.; Meyer, E.; Holm, R. H.; Nocera, D. G. *J. Am. Chem. Soc.* **2003**, *125*, 4755.
(16) Autschbach, J.; Ziegler, T. *Coord. Chem. Rev.* **2003**, *238*−*239*, 83.
(17) Casida, M. E.; Jamorski, C.; Casida, K. C.; Salahub, D. R. *J. Chem. Phys.* **1998**, *108*, 4439.
(18) Bauernschmitt, R.; Alrichs, R. *Chem. Phys. Lett.* **1996**, *256*, 454.
(19) Fabian, J.; Diaz, L. A.; Seifert, G.; Niehaus, T. *J. Mol. Struct. (THEOCHEM)* **2002**, *594*, 41.
(20) Gray, T. G.; Holm, R. H. *Inorg. Chem.* **2002**, *41*, 4211.
(21) Frisch, M. J.; Trucks, G. W.; Schlegel, H. B.; Scuseria, G. E.; Robb, M. A.; Cheeseman, J. R.; Zakrzewski, V. G.; Montgomery, J. A., Jr.; Stratmann, R. E.; Burant, J. C.; Dapprich, S.; Millam, J. M.; Daniels, A. D.; Kudin, K. N.; Strain, M. C.; Farkas, O.; Tomasi, J.; Barone, V.; Cossi, M.; Cammi, R.; Mennucci, B.; Pomelli, C.; Adamo, C.; Clifford, S.; Ochterski, J.; Petersson, G. A.; Ayala, P. Y.; Cui, Q.; Morokuma, K.; Malick, D. K.; Rabuck, A. D.; Raghavachari, K.; Foresman, J. B.; Cioslowski, J.; Ortiz, J. V.; Stefanov, B. B.; Liu, G.; Liashenko, A.; Piskorz, P.; Komaromi, I.; Gomperts, R.; Martin, R. L.; Fox, D. J.; Keith, T.; Al-Laham, M. A.; Peng, C. Y.; Nanayakkara, A.; Gonzalez, C.; Challacombe, M.; Gill, P. M. W.; Johnson, B. G.; Chen, W.; Wong, M. W.; Andres, J. L.; Head-Gordon, M.; Replogle, E. S.; Pople, J. A. *Gaussian 98, Revision A.9*; Gaussian, Inc.: Pittsburgh, PA, 1998.
(22) Becke, A. D. *Phys. Rev. A* **1988**, *38*, 3098.
(23) Perdew, J. P.; Zunger, A. *Phys. Rev. B* **1981**, *23*, 5048.
(24) Perdew, J. P. *Phys. Rev. B* **1986**, *33*, 8822.
(25) Hay, P. J.; Wadt, W. R. *J. Chem. Phys.* **1985**, *82*, 299.
(26) Couty, M.; Hall, M. B. *J. Comput. Chem.* **1996**, *17*, 1359.
(27) Hariharan, P. C.; Pople, J. A. *Theor. Chim. Acta* **1973**, *28*, 213.
(28) Francl, M. M.; Pietro, W. J.; Hehre, W. J.; Binkley, J. S.; Gordon, M. S.; DeFrees, D. J.; Pople, J. A. *J. Chem. Phys.* **1982**, *77*, 3654.
(29) Arrhenius, S. *Z. Physik. Chem.* **1889**, *4*, 226.
(30) Englman, R. *Solid State Commun.* **1983** *47*, 723.
(31) Koch, W.; Holthausen, M. *A Chemist's Guide to Density Functional Theory*; Wiley-VCH: Weinheim, 2000.
(32) Lynch, B. J.; Fast, P. L.; Harris, M.; Truhlar, D. G. *J. Phys. Chem.* **2000**, *104*, 4811.
(33) Szilagyi, R. K.; Metz, M.; Solomon, E. I. *J. Phys. Chem. A* **2002**, *116*, 2994.
(34) Szilagyi, R. K.; Solomon, E. I. *Curr. Opin. Chem. Biol.* **2002**, *6*, 250.
(35) Wilson P. J.; Tozer, D. J. *J. Chem. Phys.* **2002**, *116*, 10139.
(36) Poater, J.; Solà, M.; Duranm, M.; Robles, J. *Phys. Chem. Chem. Phys.* **2002**, *4*, 722.
(37) Abu-Awwad, F.; Politzer, P. *J. Comput. Chem.* **2000**, *21*, 227.
(38) Stratmann, R. E.; Scuseria, G. E.; Frisch, M. J. *J. Chem. Phys.* **1998**, *109*, 8218.
(39) Köstlmeier, S.; Nauslov, V. A.; Herrmann, W. A.; Rösch, N. *Organometallics* **1997**, *16*, 1786.
(40) Bosque, R.; Maseras, F.; Eisenstein, O.; Patel, B. P.; Yao, W.; Crabtree, R. H. *Inorg. Chem.* **1997**, *36*, 5505.
(41) Psaroudakis, N.; Mertis, K.; Liakos, D. G. *Chem. Phys. Lett.* **2003**, *369*, 490.
(42) Cotton, F. A.; Gu, J.; Murillo, C. A.; Timmons, D. J. *J. Chem. Soc., Dalton Trans.* **1999**, 3741.
(43) Gagliardi L.; Roos, B. O. *Inorg. Chem.* **2003**, *42*, 1599.
(44) Wilson, R. B.; Solomon, E. I. *Inorg. Chem.* **1978**, *17*, 1729.
(45) Bersuker, I. B. *Chem. Rev.* **2001**, *101*, 1067.
(46) Bersuker, I. B. *Electronic Structure and Properties of Transition Metal Compounds: Introduction to the Theory*; Wiley-Interscience: New York, 1996.
(47) Figgis, B. N.; Hitchman, M. A. *Ligand Field Theory and Its Applications*; Wiley-VCH: New York, 2000; Chapter 7, p 149.
(48) Comba, P.; Hauser, A.; Kerscher, M.; Pritzkow, H. *Angew. Chem., Int. Ed.* **2003**, *42*, 4536.
(49) Selby, H. D.; Zheng, Z.; Gray, T. G.; Holm, R. H. *Inorg. Chim. Acta* **2001**, *312*, 205.
(50) Zheng, Z.; Gray, T. G.; Holm, R. H. *Inorg. Chem.* **1999**, *38*, 4888.
(51) Willer, M. W.; McLauchlan, C. C.; Holm, R. H. *Inorg. Chem.* **1998**, *37*, 328.
(52) Zheng, Z.; Long, J. R.; Holm, R. H. *J. Am. Chem. Soc.* **1997**, *119*, 2163.
(53) Zheng, Z.; Holm, R. H. *Inorg. Chem.* **1997**, *36*, 5173.
(54) Chen, Z.-N.; Yoshimura, T.; Abe, M.; Sasaki, Y.; Ishizaka, S.; Kim, H.-B.; Kitamura, N. *Angew. Chem., Int. Ed.* **2001**, *40*, 239.
(55) Yoshimura, T.; Umakoshi, K.; Sasaki, Y.; Sykes, A. G. *Inorg. Chem.* **1999**, *38*, 5567.